Adaptive Control of an Actuated-Ankle-Foot-Orthosis

V. Arnez, H. Rifai, Yacine Y. Amirat, Samer S. Mohammed

Version of Record: https://www.sciencedirect.com/science/article/pii/S0967066118302557
Manuscript_09190cd004a3ab96ee518aa790bfa2fa

Adaptive Control of an Actuated Ankle Foot Orthosis for Paretic Patients

V. Arnez-Paniagua[a], H. Rifaï[a], Y. Amirat[a], S. Mohammed[a,*]

[a]*Laboratoire Images, Signaux et Systèmes Intelligents (LISSI), Université Paris-Est Créteil (UPEC), 94400 Vitry-sur-Seine, France*

Abstract

This paper deals with the control of an active ankle foot orthosis (AAFO) to assist the gait of paretic patients. The AAFO system is driven by both, the residual human torque delivered by the muscles spanning the ankle joint and the AAFO's actuator's torque. A model reference adaptive control is proposed to assist dorsiflexion and plantar-flexion movements of the ankle joint during level walking. Unlike most classical model-based controllers, the proposed one does not require any prior estimation of the system's (AAFO-wearer) parameters. The ankle reference trajectory is updated online based on the main gait cycle events and is adapted with respect to the self-selected speed of the wearer. The adaptive desired ankle trajectory is estimated using cubic spline interpolations between the different key events of the gait cycle. The closed-loop input-to-state stability of the AAFO-wearer system with respect to a bounded human muscular torque is proved by Lyapunov analysis. Experimental results obtained from three healthy subjects and one paretic patient, show satisfactory results in terms of tracking performance and ankle assistance throughout the full gait cycle. The experiments also show good performance at different walking speeds and with different gait sub-phase duration proportions.

Keywords: Adaptive control, actuated ankle foot orthosis, gait assistance, paretic patient, adaptive ankle joint reference

1. INTRODUCTION

Every year, a growing number of people is diagnosed with a disability that prevents them from performing smooth movements. According to the World Health Organization, a review in 2017 states that around 15% of the world's population lives with some form of disability, and 2-4% of this population experiences significant difficulties in functioning [1]. Rates of disability are increasing due to population ageing and increases in chronic health conditions, among other causes. Furthermore, disability-associated health care expenditures accounted for 26.7% of all health care expenditures for adults residing in the United States [1]. Therefore, there is an increasing interest in healthcare technologies with the emergence of new economic and industrial sectors.

Paretic patients may have different levels of impairment, e.g., some have total loss of strength to initiate a movement, while others are able to move their limbs within a limited range. The lack of strength and coordination during a gait cycle derives in pathologies and, oftentimes, the patient adapts the gait movements to circumvent the weaker limb. The differences in impairment levels require different levels of assistance. Therefore, the required therapy depends on the level of impairment, and it needs to be adjusted as the patient improves strength, coordination and achievement of certain tasks.

In conventional therapy, the patients are manually assisted by therapists, which is a difficult and painful task to be performed continuously for more than few minutes. This assistance is ideally provided in such a way that the gait cycle tends towards a healthy pattern as close as possible, while verbally asking the patient for participation and more engagement. It is still not clear yet if the robotic therapy is better than the conventional one at the same dose [2–7], but what is becoming clear is that an intense and prolonged therapy offers the best outcome in terms of patient recovery for different assessment metrics [8–10]. To reach this goal, wearable robots present a great potential due to their ability to provide precise and continuous assistance. Thus, wearable robots for rehabilitation purposes, have seen a significant increase in attention over the last decade.

Different exoskeletons have been recently developed. Some of them are dedicated to the lower limbs to train patients to recover strength and coordination by improving their walking abilities [11–15]. Such exoskeletons can be used in rehabilitation, from moving a joint in the context of static exercises, to assisting the patient at specific moments or during the whole gait cycle. The control method used for each exoskeleton has a direct impact on the level and rate of human adaptation to the active device; i.e., the central nervous system can adapt more easily to a continuous, smooth and proportionate stimulus [16]. Different control strategies have been applied to achieve such goals [15, 17, 18]. For example, in [19–21], lower limb exoskeletons are controlled based on the use of electromyography (EMG) signals to assist the patient according to an intention detection. The controllers used in these studies are proportional to the EMG signals, but the muscles working around the ankle joint could work in synergy by co-contracting at specific moments of the gait cycle, as reported in [22], thus requiring to consider more complex controllers

*Corresponding author
Email addresses:
victor.arnezpaniagua@univ-paris-est.fr (V. Arnez-Paniagua), hala.rifai@u-pec.fr (H. Rifaï), amirat@u-pec.fr (Y. Amirat), samer.mohammed@u-pec.fr (S. Mohammed)

[1] http://www.who.int/mediacentre/factsheets/fs352/en/, Accessed: 2018-01-10

for EMG-based applications. However, in practice, EMG-based approaches are usually very complex to implement as EMG signals are largely affected by sensor position, skin impedance changes, and muscular fatigue [23]. Furthermore, the residual muscular activities are difficult to measure with patients having high levels of muscle impairments. Other examples of control strategies for lower limb exoskeletons include the trajectory reference tracking in terms of lower limb kinematics (joint positions and velocities), [24–28]. These systems have the advantage of potentially being able to assist the patient disregarding the level of the impairment. However, such control strategies are based on the use of predefined trajectories that may not fit to different profiles of patients, particularly in terms of walking speed, step length, ankle range of motion, etc. An example of torque control is presented in [29], an electro-hydraulic actuated ankle foot orthosis is used to assist the walk using a constant or gait phase dependent torque fields. In [30], a force control scheme is developed in order to stretch the ankle joint in the sagittal plane for after acute stroke rehabilitation. Other control strategies adapt the stiffness, inertia or impedance of the coupled human-exoskeleton system during daily activities as function of gait phase events detection, [31–35]. These systems have the advantage of not requiring a predefined trajectory, however, they require a minimum residual voluntary effort to initiate movements and they require as well a prior identification of the human-exoskeleton parameters [35, 36]. Feedforward controllers based on the detected gait phases are presented in [37–40], where the magnitude of the assistance to the ankle joint depends on the detected gait phase. Finally, an example of a soft orthotic device is presented in [41], where a feedforward controller is used due to the complexity of the model of the system but the authors concluded that a feedback controller is required in order to achieve more accurate joint angle control.

There are several key causes of pathologies that affect the gait, e.g., spasticity [42], co-contraction of plantar flexion muscles, and muscle weaknesses, [43]. For pathologies originated by the dorsiflexor muscle group, the primary focus is on the foot-drop and the foot-slap. The former occurs during the swing phase and is due to the lack of sufficient dorsiflexion to ensure toe clearance and results in a steppage-type gait pattern. The latter occurs during the loading response sub-phase, it is caused by the uncontrolled deceleration of the toes shortly after initial contact that generally causes an audible foot slap [15]. For the pathologies originated by the plantar-flexor muscle group, the main focus is in the stance phase of the gait cycle. Limited range ankle plantar-flexors affect the gait stability and reduce the torque needed for forward progression. Therefore, patients compensate this deficiency by reducing walking speed and shortening contralateral step length.

Control schemes are customized to the pathology characteristics and mechanical configuration of the device [18]. For example, there are several actuated ankle foot orthosis (AAFO) that are able to provide assistive torque only in the dorsiflexion direction to prevent foot drop and foot slap [41], or plantarflexion direction to promote a more effective foot push-off power before the swing phase [35]. Other AAFOs are able to produce torque in both directions of the sagittal plane of the ankle joint, effectively assisting during push-off at the end of the stance phase, as well as providing assistance during the swing phase to prevent from foot drop. They can decide the magnitude and direction of the assistance by pre-selecting the assistive torque at each identified gait phase [17, 29, 37–39], as a function of EMG signals [21], or as a function of the error between the current ankle joint profile and a reference [25–28]. Finally, there are some examples of semi-active devices that can control the stiffness or damping of the orthotic device in order to facilitate a controlled deceleration of the toes during the loading response sub-phase of the gait, increase dorsiflexion during the swing phase [32]. It is worth mentioning, that only [20, 26, 30, 32, 37] present results of tests with non-able bodied subjects, while the rest of them have tested the systems with healthy subjects only. Furthermore, [21, 25, 26, 38, 40] present systems that actively assist through the whole gait cycle while the rest of the systems are assisting during specific gait phases or are not used in walking applications.

In this work, an AAFO is used to assist the wearer through the whole gait cycle by using a model reference adaptive controller. This control approach has the advantage of not requiring a previous system's parameters identification process and can adjust to the human-AAFO system changes in real time. Furthermore, an adaptive reference trajectory is proposed as a function of the walking speed of the wearer and the identification of the transitions between the different gait sub-phases. This adaptation of the reference trajectory avoids the use of a unique predefined trajectory of the ankle joint. It also allows the wearer focusing on the task and not on the synchonization with the reference trajectory neither via audible nor visual cues. The proposed approach was implemented with three healthy subjects and one paretic patient to assess the effectiveness of the adaptive ankle reference generator algorithm and the adaptive controller.

In a previous work [44], an adaptive control for an actuated ankle foot orthosis was introduced. This controller was further studied in [45] by bounding the adaptive parameters of the controller. The former controller was generating assistive torque during the swing phase of the gait in order to prevent foot drop. The latter controller was able to assist during the whole gait cycle. The stability of the system was studied for both controllers with a Lyapunov function for the scenarios where the human muscles spanning the ankle joint are passive (not exerting torque) or active (exerting torque). Furthermore, the ability of the system to assist the gait during the swing phase for the first controller and during the whole gait cycle for the second one was evaluated with one healthy subject. The present study extends these previous works in manyfold; firstly, by using an adaptive ankle joint angle profile as the reference; secondly, by applying assistive torque during the whole gait cycle; thirdly, by assessing the stability and tracking performance of the human-AAFO system with three healthy subjects; and fourthly, by assessing the ability of the system to assist the gait of a paretic patient.

The paper is structured as follows. In section 2, the generation of the adaptive reference trajectory is presented. In

section 3, the model of the AAFO system is shown. In section 4, the adaptive controller is developed. In section 4.2, the stability analysis is provided. In section 5, a description of the robot and the experimental setup are presented. In section 6, the experimental results are presented followed by a discussion in section 7.

2. ADAPTIVE ANKLE REFERENCE GENERATOR

In this section, an adaptive ankle reference generator (AARG) algorithm is presented. First, the gait cycle is described as well as the sensors used to detect the different gait sub-phases. The ankle reference trajectory is updated as a function of the real-time gait cycle temporal evolution, in particular, the step duration and the repartition of the gait sub-phases.

2.1. Gait cycle

The gait cycle can be divided in two main phases, as defined by Winter [46]: the stance and the swing phases, as it is shown in Figure 1. Each gait cycle is characterized by specific events such as initial contact (IC), toe landing (TL), heel off (HO), toe off (TO), and maximum dorsiflexion (MD) during the swing phase. The stance phase of the gait cycle can be divided into several sub-phases that are: loading response (LR), mid-stance (MS), which can be further divided in early-mid-stance (EMS) and late-mid-stance (LMS), terminal stance (TS), and pre-swing (PS). Similarly, the swing phase can be divided into several sub-phases based on the analysis of the opposite foot that is in contact with the ground. These sub-phases are: initial swing (ISw), mid-swing (MSw), and terminal swing (TSw).

By detecting specific events during the stance phase, it is possible to determine the key moments at which the ankle joint angle profile switches from dorsiflexion to plantar-flexion and vice-versa as it is shown in Figure 1. Particularly, during the swing phase, the ankle joint rises the foot to avoid foot-drop, and anticipates the foot for the IC event. The standing foot terminates the stance phase with a push-off movement and then dorsiflexes the ankle joint to the maximum dorsiflexion (MD) value and then remains dorsiflexed until the IC event. The time needed by the ankle joint to reach the MD varies from one subject to another. Generally, the MD happens around the 62% of the swing phase duration, that is about 85% of the whole gait cycle.

In order to detect the key moments, three force sensitive resistors (FSR) are placed in each of the insoles of both feet, Figure 2. Moreover, one Inertial Measurement Unit (IMU) is placed at the shank level of the left leg to measure the acceleration of the shank along the longitudinal axis. This IMU participates as well in accurately detecting the IC event.

2.2. Gait detection

A Mamdani fuzzy inference system has been developed to detect the gait sub-phases based on the outputs of the FSR sensors [39, 47]. The algorithm detects the eight sub-phases

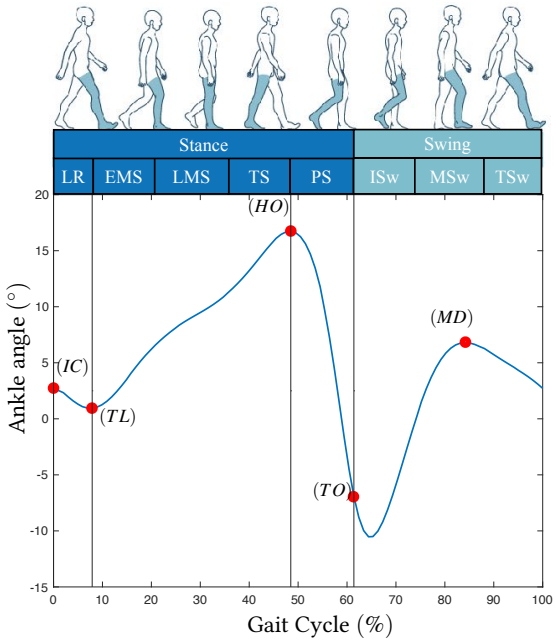

Figure 1: On the top, the description of the gait by means of the gait sub-phases (LR=Loading Response, EMS=Early Mid-Stance, LMS=Late Mid-Stance, TS=Terminal Stance, PS=Pre-Swing, ISw=Initial Swing, MSw=Mid-Swing, TSw=Terminal Swing). On the bottom, the events in the gait cycle that trigger a transition of gait sub-phases or that describe a relative minimum or maximum in the ankle joint angle profile. The ankle angle is measured from the relaxed ankle angle, such that the positive values are considered dorsiflexion and the negative values are plantar-flexion.

including the five sub-phases during the stance phase; the remaining three sub-phases during the swing phase are approximately estimated. The human gait is analysed through all the sub-phases where the each sub-phase's likelihood of occurrence is determined using a standard fuzzy membership value (μ).

Let $\vec{F}_{tj}$ be the vector that contains the acquired data for a given FSR sensor j from the beginning of a session till a given time t. The configuration of the FSR sensors is presented in Figure 2, where $j \in \{1,\dots,6\}$ shows the left heel, left middle, left toes, right heel, right middle, and right toes sensors, respectively. The range in the magnitude of the signal for each sensor j is given by:

$$r_j = max(\vec{F}_{tj}) - min(\vec{F}_{tj}), \tag{1}$$

where max$(\cdot)$ and min$(\cdot)$ represent the maximum and minimum values of the enclosed vector. Let N_j be the threshold value for each sensor j such that:

$$N_j = r_j \cdot h + min(\vec{F}_{tj}), \tag{2}$$

where h is the threshold percentage, an empirical value of 5% was found to be effective ($h = 0.05$). The membership function f_j for each sensor j is given by:

$$f_j = \frac{1}{2}\left(\tanh\left(\frac{k_j(F_{tj} - N_j)}{r_j} - 1\right) + 1\right), \tag{3}$$

where k_j represents the gain for each sensor j, and F_{tj} the measurement output of each FSR sensor j at a given time t

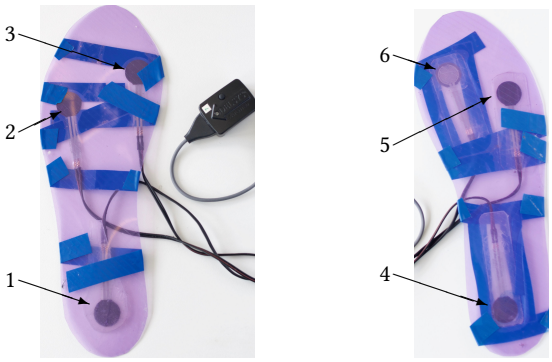

(a) Left insole. (b) Right insole.

Figure 2: The insoles with the force sensitive resistors (FSR). Each sensor is labeled with the number used in the equations.

during the session. Effective values for k_j were empirically tuned and were set to $k_{1,2,3} = 3$ and $k_{4,5,6} = 4$. This was done by increasing the sensibility gain k_j of each membership function f_j until every gait phase could be detected during level walking done by a healthy subject. Furthermore, once these values are set, they allow the detection of each gait phase in a healthy gait pattern. However, if a paretic patient with a gait pathology would use the system, it would be expected that some gait phases are not executed and therefore not detected. Consequently, once the sensibility gains k_j are set and tested with the healthy subjects, these values are not changed for the paretic patient. Given that the paretic limb of the patient might not produce a normal ground reaction force (GRF) pattern, two FSR sensors are used to measure the GRF of the left toes, then the membership functions for the left middle and toes FSR sensors (f_2 and f_3) are processed by selecting the maximum value of the two FSRs. The fuzzy membership value (FMV) is calculated for each sub-phase as follows:

$$\begin{aligned}
\mu_{LR} &= min(f_1, 1 - max(f_2, f_3), 1 - f_4, f_6), \\
\mu_{EMS} &= min(f_1, 1 - max(f_2, f_3), 1 - f_4, 1 - f_6), \\
\mu_{LMS} &= min(f_1, max(f_2, f_3), 1 - f_4, 1 - f_6), \\
\mu_{TS} &= min(1 - f_1, max(f_2, f_3), 1 - f_4, 1 - f_6), \\
\mu_{PS} &= min(f_1, f_4), \\
\mu_{ISw} &= min(1 - f_1, 1 - max(f_2, f_3), f_4), \\
\mu_{MSw} &= min(1 - f_1, 1 - max(f_2, f_3), 1 - f_4, f_5), \\
\mu_{TSw} &= min(1 - f_1, 1 - max(f_2, f_3), 1 - f_4, f_6).
\end{aligned} \tag{4}$$

Afterwards, the sub-phase with the maximum FMV value is selected. Finally, to increase accuracy in the detection of the IC event, an additional IMU is placed at the shank level. If the TSw sub-phase is detected and the magnitude of the acceleration, measured by the IMU in the shank, crosses a certain threshold ($a_{shank} > -11 m/s^2$), the LR sub-phase is considered to have occurred instead. The threshold value of $11 m/s^2$ was empirically chosen from experiments. Adding an additional IMU has considerably improved the results of detecting the IC event than simply using the FSR sensors.

By calculating the duration of each sub-phase and the duration of each step, it is possible to calculate in real time the duration percentage of each sub-phase with respect to the gait cycle, and the time between the gait events. At any given step, the average duration percentage for each sub-phase is calculated from the last five steps. The gait duration is then updated eight times per gait cycle, one time per sub-phase detected. The average duration percentage of each sub-phase is obtained after the first five steps and is then updated after each sub-phase detection.

2.3. Adaptive reference generator

The reference trajectory is based on an ankle joint angle profile that has been obtained from analyzing the gait of 20 healthy subjects. The gait analysis has been performed in a clinical environment using a motion capture system (Motion Analysis Corporation, Santa Rosa, CA, USA, six cameras, Sampling Frequency 100 Hz) and two force plates (AMTI, Watertown, MA, USA, Sampling Frequency 1000 Hz), for more details please refer to [48]. Based on this profile, the ankle joint angle values, defined as key points, of the IC, TL, HO, TO, and MD events have been extracted and are shown in Table 1.

The adaptive reference trajectory is calculated at the moment of the occurrence of any of the aforementioned events using a cubic spline function, if no event is detected, the previously calculated reference trajectory is followed, as shown in the flow chart in Figure 3a. To update the reference trajectory, the beginning of the cubic spline function is the current reference ankle joint angle, and it is calculated until reaching the next key point value in the gait cycle. For example, if the TL event is detected, a cubic spline trajectory that connects the current value of the ankle joint angle reference to the HO key point value is calculated. The duration of the cubic spline is defined by the duration of the sub-phases involved between the initial and final events conforming the cubic spline. In the given example, the duration of the cubic spline is the sum of the duration of the MS and TS sub-phases. The current ankle joint velocity reference is used as the initial condition for the cubic spline, and an ankle joint velocity value of zero is used as the final condition. This process for updating the ankle joint reference profile is illustrated in the flow chart in Figure 3b. The adaptive reference ankle joint angular velocity and accelerations are calculated afterwards by numerically deriving the calculated cubic spline trajectory. In the case where the cubic spline trajectory is completed before the next event occurs, the ankle joint reference profile remains at the last value of the cubic spline until the next event is detected and the process continues. For the swing phase, if the TO event is detected, the cubic spline is calculated from the current ankle joint angle reference, then follows the MD key point in the middle of the path, and ends with the IC event.

With this approach, the AARG calculates paths connecting the main key points of some average healthy ankle profile and

Table 1: *Key point values extracted from the average gait cycle of 20 healthy subjects.*

	IC (°)	TL (°)	HO (°)	TO (°)	MD (°)
Ankle angle θ	2.7	0.95	16.74	-6.92	6.8

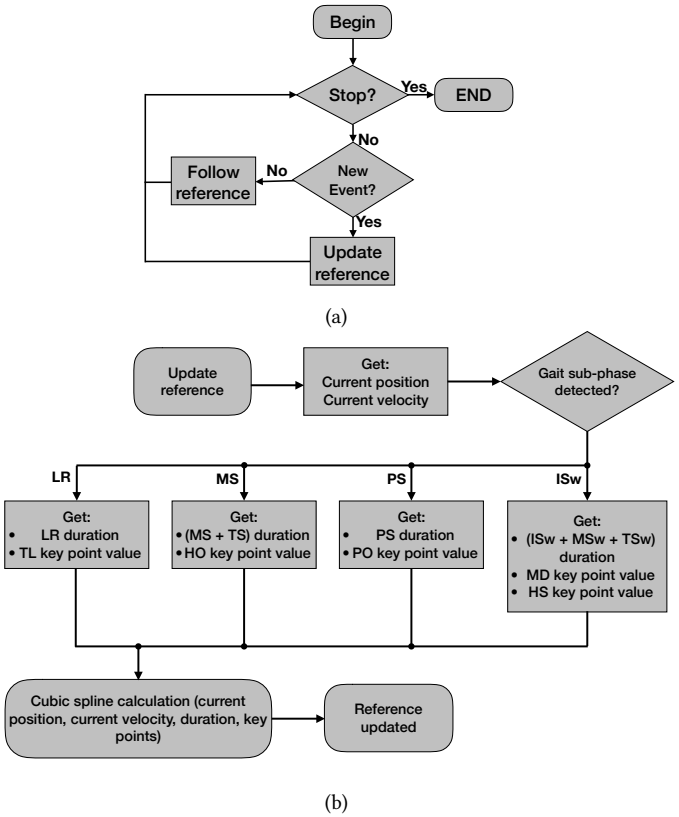

Figure 3: On the top, the flow chart for the ankle reference generator program. On the bottom, the flow chart for the ankle reference update program.

updates the adaptive reference trajectory after the detection of each of the main gait events. The advantage of this algorithm is that it does not impose any specific walking speed to the wearer but rather adapts to the generated desired kinematic trajectory as a function of the sub-phase durations. The wearer is then following a desired ankle joint angle completely adapted to his/her gait cycle and subphases duration. Furthermore, the wearer is required to be engaged in the walking activity in order to generate the trajectory, which is an important feature in the rehabilitation process.

3. SYSTEM MODELING

The orthosis used in this study is an AAFO attached to the subject's left leg, by means of straps to fix the robot to the calf and thigh, as shown in Figure 4. The orthosis has one active and one passive degrees of freedom (DoF), at the ankle and the knee joints, respectively. The active DoF is driven by a DC motor and a gearbox with a gear ratio of 114.4:1. The AAFO can be backdriven by the wearer during walking and it is considered as rigidly fixed to the subject's leg. The foot and the AAFO are considered as one unit referred to as the AAFO system. In this study, the problem of misalignment between the ankle joint and the AAFO's rotational axis when donning the device has been considerably reduced by adjusting manually the orthosis to every wearer's morphology using adaptable straps as shown in Fig. 6a. Special care has been taken during experiments in

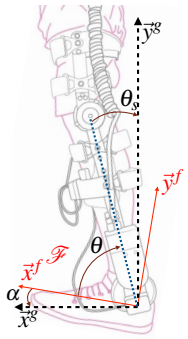

Figure 4: The angles determining the foot and the shank orientations. Foot frame $\mathscr{F}(\vec{x}^f, \vec{y}^f, \vec{z}^f)$, where $\vec{x}^f$ is in the same plane as the heel-half of the insole. Ground frame $\mathscr{G}(\vec{x}^g, \vec{y}^g, \vec{z}^g)$.

order to avoid reaching the full ankle joint flexion/extension which considerably reduce the joint misalignment.

In order to model the AAFO system, a frame $\mathscr{F}(\vec{x}^f, \vec{y}^f, \vec{z}^f)$ is considered fixed to the left foot such that $\vec{x}^f$ has the same direction as the foot while the origin is located at the ankle joint. $\vec{z}^f$ is defined as the rotational axis of the ankle joint. $\vec{y}^f$ is defined such that the three-sided frame $\mathscr{F}$ is direct. A second frame $\mathscr{G}(\vec{x}^g, \vec{y}^g, \vec{z}^g)$ is placed at the ground, with $\vec{x}^g$ parallel to the horizontal, $\vec{y}^g$ parallel to the vertical, and $\vec{z}^g$ defined such as the three-sided frame $(\vec{x}^g, \vec{y}^g, \vec{z}^g)$ is direct. Note that $\vec{z}^f$ and $\vec{z}^g$ are collinear.

Denote by θ the angle between the foot and the shank, by θ_s the angle between the shank and the vertical axis and by α the angle between the foot and the horizontal axis (Figure 4). Using the embedded encoders in the AAFO and IMUs, θ and θ_s are accessible to measurement and α is given by $\alpha = \theta + \theta_s - \frac{\pi}{2}$.

Several torques acting on the AAFO system at the ankle level are being considered. The AAFO system's dynamics can be expressed as follows:

$$J\ddot{\theta} = \tau_f + \tau_a + \tau_s + \tau_r + \tau_{gravity} + \tau_h + \tau, \tag{5}$$

where τ_f is the friction torque (solid and viscous), τ_a is the torque induced by the translational acceleration of the foot, τ_s is the system's joint stiffness torque, τ_r is the torque induced by the ground reaction forces, $\tau_{gravity}$ is the gravity torque exerted by the foot on the ankle, τ_h is the torque produced by the plantar flexion and dorsiflexion muscle groups, and τ is the torque developed by the AAFO's actuator. All the torques are considered positive if they induce a counter clockwise rotation. The definitions of the system's parameters are detailed in Table 2.

Each of the aforementioned torques is defined as follows:

$$\begin{aligned} \tau_f &= -A\,\mathrm{sign}\dot{\theta} - B\dot{\theta}, \\ \tau_a &= -C(a_y \cos\alpha - a_x \sin\alpha), \\ \tau_s &= -K(\theta - \theta_r), \\ \tau_r &= -\gamma(R_1 x_1 - R_2 x_2 - R_3 x_3)\cos\alpha, \\ \tau_{gravity} &= -\tau_g \cos\alpha. \end{aligned} \tag{6}$$

Note that the system's parameters A, B, C, K, γ, and τ_g are not necessarily constant. In fact, some of them are functions

Table 2: *Nomenclature*

Symbol	Description
θ_s	Angle between the shank and the vertical axis
α	Angle between the foot and the horizontal axis
$\theta, \dot{\theta}, \ddot{\theta}$	Ankle joint angle, angular velocity and acceleration
$\tilde{\theta}, \dot{\tilde{\theta}}$	Ankle joint angle and angular velocity errors
θ_r	Ankle joint angle at the rest position of the foot
J	System's moment of inertia
A	System's solid friction coefficient
B	System's viscous friction coefficient
K	System's stiffness coefficient
τ_g	System's gravity torque coefficient
γ	System's ground reaction torque coefficient
C	System's acceleration torque coefficient
a_x, a_y	Longitudinal and vertical linear accelerations
R_1, R_2, R_3	GRF at the heel, middle and toes levels
x_1, x_2, x_3	Positions of the FSR in $\vec{x}^f$ direction
τ	Control torque
τ_h	Human muscular torque actuating the ankle joint
sign$(\cdot)$	Signum function
κ	Scalar positive gain
λ	Scalar positive parameter

of different variables, e.g., the stiffness coefficient K could be approximated by a musculoskeletal model of the ankle joint as a function of the muscle groups activation [49]. However, the effects of these parameter's variations are considered as external perturbations and are included in the human torque variable τ_h. Consequently, these parameters are considered constant for this study.

Also, the FSR sensors signals of the contralateral foot (R_1, R_2, and R_3) multiplied by the distance from the ankle joint to the sensor in the $\vec{x}^f$ direction (x_1, x_2, and x_3) generates an estimation of the GRF. Although this estimation can be improved by adding more sensors in the insole, doing so would yield in a bulky system, which require further computational time. It was a fair tradeoff between the GRF estimation and the computational time to use three sensors. This has the further advantage of not requiring more FSR sensors than those already used for the gait detection algorithm described in section 2.2. These inaccuracies in the estimation of the system's parameters will be treated using an adaptive controller, described in section 4.

By replacing (6) in (5), we obtain:

$$\begin{aligned} J\ddot{\theta} = &-A\text{sign}\dot{\theta} - B\dot{\theta} - C(a_y\cos\alpha - a_x\sin\alpha) \\ &- K(\theta-\theta_r) - \gamma(R_1x_1 - R_2x_2 - R_3x_3)\cos\alpha \\ &- \tau_g\cos\alpha + \tau_h + \tau. \end{aligned} \tag{7}$$

Remark 1. *The human torque τ_h is generated by the muscles actuating the ankle joint and is considered to be bounded by Δ_h: $|\tau_h| \leq \Delta_h$.*

4. ADAPTIVE CONTROLLER

The AAFO system defined in (7) depends on the parameters defined in (6). Each of these parameters depend on the individual foot's and the orthosis' parameters. While the orthosis' parameters can be identified once, the foot's parameters depend on the subject and should be identified at the beginning of every experiment. Moreover, the foot's parameters are subject to changes during the experiment, e.g., due to the subject's muscular fatigue. To avoid an identification process prior to the experiments, which is often a complex task, the approach adopted in this work is based on the use of an adaptive controller to drive the ankle joint angle towards the desired trajectory generated using the adaptive reference generator shown in section 2.3. The block diagram of the closed-loop system is shown in Figure 5. Let θ_d, $\dot{\theta}_d$ and $\ddot{\theta}_d$ be the desired angle, angular velocity and acceleration of the ankle joint respectively. Define

$$s = \dot{\tilde{\theta}} + \lambda\tilde{\theta}, \tag{8}$$

where λ is a scalar positive parameter; $\tilde{\theta}$ and $\dot{\tilde{\theta}}$ are the position and velocity errors respectively ($\tilde{\theta} = \theta - \theta_d$, $\dot{\tilde{\theta}} = \dot{\theta} - \dot{\theta}_d$).

Assumption 1. *The current and desired ankle joint angle values and their derivatives up to the second order (θ, $\dot{\theta}$, $\ddot{\theta}$, θ_d, $\dot{\theta}_d$, $\ddot{\theta}_d$) are assumed known and bounded.*

The proposed adaptive control torque is applied during the whole gait cycle. It has the following expression:

$$\begin{aligned} \tau = &\hat{J}(\ddot{\theta}_d - \lambda\dot{\tilde{\theta}}) + \hat{A}\text{sign}\dot{\theta} + \hat{B}\dot{\theta} + \hat{K}(\theta-\theta_r) \\ &+ \hat{C}(a_y\cos\alpha - a_x\sin\alpha) + \hat{\tau}_g\cos\alpha - \kappa s \\ &+ \hat{\gamma}(R_1x_1 - R_2x_2 - R_3x_3)\cos\alpha, \end{aligned} \tag{9}$$

where κ is a scalar positive gain and $\hat{J}$, $\hat{A}$, $\hat{B}$, $\hat{K}$, $\hat{C}$, $\hat{\tau}_g$, and $\hat{\gamma}$ are respectively the estimated torque coefficients for the inertia, solid and viscous friction, stiffness, acceleration, gravity, and ground reaction. The parameters adaptation law is given by:

$$\begin{aligned} \dot{\hat{A}} &= -a_1\text{sign}\dot{\theta}s, \\ \dot{\hat{B}} &= -a_2\dot{\theta}s, \\ \dot{\hat{C}} &= -a_3(a_y\cos\alpha - a_x\sin\alpha)s, \\ \dot{\hat{K}} &= -a_4(\theta-\theta_r)s, \\ \dot{\hat{J}} &= -a_5(\ddot{\theta}_d - \lambda\dot{\tilde{\theta}})s, \\ \dot{\hat{\gamma}} &= -a_6(R_1x_1 - R_2x_2 - R_3x_3)\cos\alpha s, \\ \dot{\hat{\tau}}_g &= -a_7\cos\alpha s, \end{aligned} \tag{10}$$

where a_i, $i \in \{1,\ldots,7\}$ are positive scalar gains. Let P be a system's parameter such that $P \in \{A,B,C,K,J,\gamma,\tau_g\}$ and $\hat{P}$ the estimated value, $\hat{P} \in \{\hat{A},\hat{B},\hat{C},\hat{K},\hat{J},\hat{\gamma},\hat{\tau}_g\}$. The parameter's estimation error is then defined as: $\tilde{P} = P - \hat{P}$ and its derivative $\dot{\tilde{P}} = -\dot{\hat{P}}$. Applying the adaptive control torque (9) to the AAFO system modeled by (7), the dynamics of the closed loop system during the whole gait cycle can be determined as follows:

$$\begin{aligned} J\dot{s} = &-\tilde{J}(\ddot{\theta}_d - \lambda\dot{\tilde{\theta}}) - \tilde{\tau}_g\cos\alpha - \tilde{C}(a_y\cos\alpha - a_x\sin\alpha) \\ &- \tilde{K}(\theta-\theta_r) - \tilde{A}\text{sign}\dot{\theta} - \tilde{B}\dot{\theta} \\ &- \tilde{\gamma}(R_1x_1 - R_2x_2 - R_3x_3)\cos\alpha - \kappa s + \tau_h. \end{aligned} \tag{11}$$

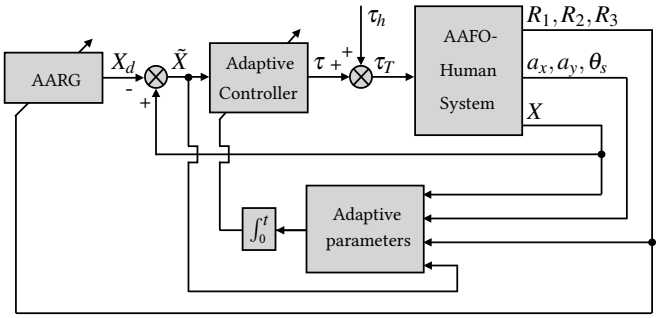

Figure 5: System's block diagram; where X, X_d and $\tilde{X}$ are respectively the current, the desired and the error stqte vectors.

Remark 2. *The purpose of the controller gains λ and κ is to adjust the response of the motor torque as a function of the position and velocity errors. While the scalar gains of the adaptive law a_i adjust the convergence speed of the estimated torque coefficients $\hat{J}$, $\hat{A}$, $\hat{B}$, $\hat{K}$, $\hat{C}$, $\hat{\tau}_g$, and $\hat{\gamma}$. These scalar gains need to be tuned manually as opposed to the system's parameters defined in (6).*

4.1. Tuning of the controller gains

In practice, the tuning of the controller's parameters (κ and λ) defined in (9), and the gains of the adaptive law (a_i, $i \in \{1, \ldots, 7\}$) defined in (10), is done with the following protocol:

1. The mean ankle joint angle profile from the 20 healthy subjects is used as the desired trajectory, see [48] for more details.
2. A healthy subject seats on a chair without exerting a muscular torque at the ankle joint level ($\tau_h = 0$), with no contact with the ground ($R_1 = R_2 = R_3 = 0$), and the adaptive gains set to zero ($a_i = 0$, $i \in \{1, \ldots, 7\}$).
3. The values of the controller gains κ and λ are initialized to small values ($\kappa = 0.2$ and $\lambda = 1$). Then, they are slowly increased manually to reduce the tracking error with a trial and error approach.
4. The wearer walks on a treadmill at a fixed speed of 2 Kilometers per hour.
5. The adaptive gains (a_i) are initialized to zero and then their values are gradually adjusted, one by one, to improve the tracking performance without compromising the system's safety and the comfort of the wearer.

This protocol is used for the first healthy subject and the resulting values of the controller gains are used for the rest of the healthy subjects. The κ and λ gains are reduced slightly for the paretic patient to limit the maximum assistance torque for safety purposes.

4.2. Stability analysis

In this section, the stability analysis of the closed-loop AAFO system is presented for two conditions; i.e. passive and active wearers.

Proposition. Consider the AAFO system modeled by (7) and assume that θ and θ_d and their derivatives up to the second order are bounded (Assumption 1). Applying τ, defined in (9), with the adaptation law defined in (10), ensures that the equilibrium point $\tilde{x} = [\tilde{\theta},\ \dot{\tilde{\theta}}]^T = [0,\ 0]^T$ is:

1. asymptotically stable when the wearer is completely passive at the ankle joint level ($\tau_h = 0$),
2. input-to-state stable with respect to the wearer's muscular torque τ_h, assuming $|\tau_h| \leq \Delta_h$ (Remark 1).

Proof. Consider the Lyapunov function V defined by:

$$\begin{aligned} V =& \frac{1}{2}Js^2 + \frac{1}{2a_1}\tilde{A}^2 + \frac{1}{2a_2}\tilde{B}^2 + \frac{1}{2a_3}\tilde{C}^2 + \frac{1}{2a_4}\tilde{K}^2 \\ &+ \frac{1}{2a_5}\tilde{J}^2 + \frac{1}{2a_6}\tilde{\gamma}^2 + \frac{1}{2a_7}\tilde{\tau_g}^2 + \kappa\lambda\,\tilde{\theta}^2. \end{aligned} \tag{12}$$

The derivative of V is given by:

$$\begin{aligned} \dot{V} =& sJ\dot{s} - \frac{1}{a_1}\tilde{A}\dot{\hat{A}} - \frac{1}{a_2}\tilde{B}\dot{\hat{B}} - \frac{1}{a_3}\tilde{C}\dot{\hat{C}} - \frac{1}{a_4}\tilde{K}\dot{\hat{K}} - \frac{1}{a_5}\tilde{J}\dot{\hat{J}} \\ &- \frac{1}{a_6}\tilde{\gamma}\dot{\tilde{\gamma}} - \frac{1}{a_7}\tilde{\tau_g}\dot{\tilde{\tau}}_g + 2\kappa\lambda\,\tilde{\theta}\dot{\tilde{\theta}}. \end{aligned} \tag{13}$$

Replacing (10) and (11) into (13), the derivative of the Lyapunov function becomes:

$$\dot{V} = -\kappa s^2 + 2\kappa\lambda\,\tilde{\theta}\dot{\tilde{\theta}} + \tau_h s, \tag{14}$$

where s is defined in (8). Replacing (8) into (14), then $\dot{V}$ becomes:

$$\dot{V} = -\kappa\dot{\tilde{\theta}}^2 - \kappa\lambda^2\tilde{\theta}^2 + \tau_h(\dot{\tilde{\theta}} + \lambda\,\tilde{\theta}). \tag{15}$$

For the condition where the wearer is passive ($\tau_h = 0$), the derivative of the Lyapunov function is:

$$\dot{V} = -\kappa\dot{\tilde{\theta}}^2 - \kappa\lambda^2\tilde{\theta}^2. \tag{16}$$

Therefore, the Lyapunov function defined in (12) is strictly decreasing. Based on Assumption 1, the errors of the ankle joint angle and its velocity ($\tilde{\theta}$ and $\dot{\tilde{\theta}}$) are bounded. Therefore, the second derivative of the Lyapunov function ($\ddot{V}$) is bounded and (16) is uniformly continuous. Using Barbalat Lemma [50], the equilibrium point $\tilde{x} = [\tilde{\theta},\ \dot{\tilde{\theta}}]^T = [0,\ 0]^T$ is asymptotically stable [51]. Consequently, θ tracks θ_d while θ and $\dot{\theta}$ remain bounded.

Since $\tilde{\theta}$ and $\dot{\tilde{\theta}}$ converge to zero then s, defined in (8), and the adaptive parameters dynamics, defined in (10), converge also to zero. Therefore, the controller's parameters converge to constant values.

For the case where the wearer is active ($\tau_h \neq 0$), the derivative of the Lyapunov function (15) can be bounded as follows:

$$\dot{V} \leq -\kappa|\dot{\tilde{\theta}}|^2 - \kappa\lambda^2|\tilde{\theta}|^2 + \tau_h(|\dot{\tilde{\theta}} + \lambda\,\tilde{\theta}|).$$

It can be verified that $|\dot{\tilde{\theta}} + \lambda\,\tilde{\theta}| \leq \sqrt{1+\lambda^2}||\tilde{x}||$, where $||\tilde{x}|| = \sqrt{\tilde{x}_1^2 + \tilde{x}_2^2}$ represents the second order Euclidean norm. Let $m = \min(1, \lambda^2)$.

$$\begin{aligned} \dot{V} &\leq -\kappa m||\tilde{x}||^2 + \tau_h\sqrt{1+\lambda^2}||\tilde{x}||, \\ &\leq -\kappa m(1-\delta)||\tilde{x}||^2 - \kappa m\delta||\tilde{x}||^2 + \tau_h\sqrt{1+\lambda^2}||\tilde{x}||, \end{aligned}$$

therefore

$$\dot{V} \leq -\kappa m(1-\delta)||\tilde{x}||^2 \quad \forall\, ||\tilde{x}|| \geq \frac{\tau_h\sqrt{1+\lambda^2}}{\kappa m\delta}, \qquad (17)$$

where $0 < \delta < 1$. In view of (12) and (17) and the asymptotic stability of the free moving AAFO's states, the system is input-to-state stable with respect to the bounded external input τ_h with $\Gamma(r) = \frac{r\sqrt{1+\lambda^2}}{km\delta}$ [50].

5. EXPERIMENTAL SETUP

In this section, the efficiency of the ankle reference trajectory generator algorithm and the effectiveness of the AAFO controller to assist patients during gait cycles are assessed through real-time experiments. Three healthy subjects wearing the AAFO and walking on a treadmill and one paretic patient walking on level ground have participated to the experiments. All healthy and patient subjects were informed of the experimental protocols and gave their consent before participating in the experiments that were approved by the department of Neurorehabilitation at Henri Mondor University Hospital. All precautions were taken to not adversely affect the health of the participants who served as research subjects. Precautions were also taken to protect the privacy of the subjects and the confidentiality of their personal information. All the three healthy subjects were able to perform complete dorsiflexion and plantar flexion of the ankle joint with no spasticity or contracture. The paretic patient presented a unilateral foot drop condition with a reduced range of motion in the plantar flexion direction during the second half of the stance phase. The patient also had an absence of strongly manifesting spasticity and co-contracture in lower extremity joints. To guarantee the safety of the subject while walking, the mechanical design of the AAFO ensures an ankle joint movement within a limited range. This range limit is set to -32° for the dorsiflexion and 22° for the plantar flexion. The subject's characteristics are presented in Table 3.

The objectives of testing the system with healthy subjects are: 1) to prove that the system is able to modify the natural ankle joint profile at targeted moments of the gait cycle with a high level of repeatability, 2) to guarantee the safety of the wearer during experiments, and 3) to evaluate the accuracy of the AARG algorithm. The experiments with the healthy subjects have been performed according to the following scenario. At first, each subject performs 4 sessions at different walking speeds with no assistance in order to validate the reference trajectory generator. Since the system is intended to modify the ankle joint profile of the healthy subjects, the IC, TL, HO, TO, and MD key points values for the AARG algorithm are set to generate an ankle joint profile different from the healthy profile. These new IC, TL, HO, TO, and MD key point values are the same for every subject and are shown in Table 4. Note that these values are different from those in Table 1, the reason is that the objectives for the healthy and paretic subjects are different. For the healthy subjects, the objective is to prove that the AAFO system is able to modify the normal ankle profile during walking. For the paretic patients, the objective is to improve the ankle profile by reducing the effects of ankle joint deficiencies during walking. Afterwards, each subject undertakes a series of sessions at a self-selected step duration with the AAFO assistance. A session, lasting 60 seconds, starts when the ankle joint angle reference generator algorithm is stable, i.e. after 5 steps. Three sessions per subject are performed to evaluate the repeatability and the consistency of the results. A resting time of 60 seconds between the sessions is provided. Finally, three more sessions per subject are performed without the AAFO's assistance in order to compare the results with those recorded during the assistance sessions. Experiments with the healthy subjects were done prior to the experiments with the paretic patient.

Table 3: *Subject's characteristics*

Subject	Gender	Age (years)	Weight (Kg)	Height (cm)
1	Male	30	63	180
2	Male	25	64	175
3	Male	27	67	185
Paretic	Female	57	50	160

Table 4: *Experimental ankle joint angle key points values in degrees (°) for the AARG.*

	IC(°)	TL(°)	HO(°)	TO(°)	MD(°)
Healthy subjects	-1	-3	6	-8.5	0
Paretic patient	-8	-13	3	-16.5	1

One further experiment with a paretic patient was also conducted. The experiment was performed under the supervision of medical staff at the Henri Mondor hospital, Créteil, France. The scenario for the experiment is as follows: Initially, the patient wears the AAFO and walks on level without the orthosis assistance for the calibration process. The ankle joint angle is measured in order to define the values for the IC, TL, HO, TO, and MD key points needed for the AARG. The purpose of the selection of the key points values is to reduce the probability of foot-drop during the swing phase by increasing the dorsiflexion angle, and to increase the push-off force during the pre-swing sub-phase by increasing the plantar-flexion angle. The resulting ankle joint angle reference has an increased dorsiflexion value during the loading response, mid-stance, terminal stance and swing phase, specially during the second half the last one, and an increased push-off plantar flexion angle during the pre-swing sub-phase. The values of the IC, TL, HO, TO, and MD key points used are shown in Table 4. The values shown in Table 1 were found to be unconfortable for the patient. Afterwards, 3 sessions without assistance and 3 sessions with assistance are conducted. All sessions are performed at a slow self-selected walking speed for improved safety and to generate an ankle joint angle profile consistent with the one produced by healthy subjects walking at 2 meters per second. One session consists of an 8 meters walking on level ground with the first 5 steps used to calibrate the AARG. A resting period of 1 minute is provided between sessions.

Figure 6 shows the setup for the experiments, illustrating the location of the IMU sensors and the actuated orthosis. The AAFO is equipped with an incremental encoder to measure the angle θ between the foot and the shank. The angular velocity of the ankle joint $\dot{\theta}$ is derived and filtered numerically with a lowpass, fourth order Butterworth filter with a cut-off frequency of 50 Hertz. Two inertial measurement units (XSENS) are also used: the first one is used to estimate the angle θ_s between the shank and the vertical axis and the second one is used to measure the translational accelerations at the ankle level a_x, a_y in the horizontal and vertical directions, respectively. Note that the gravitational acceleration has been removed from the measurement of the accelerations a_x and a_y. Six FSR are embedded in the left and right insoles and are connected to a wireless system (Trigno, Delsys), as seen in Figure 2. During the experiments, a gait cycle was measured from the initial heel contact of one foot to the next initial heel contact of the same foot. All data were time normalized to 100% of the gait cycle. The ankle joint angle has been resampled at 2000 samples per gait cycle, so that each point represents 0.05% of the gait cycle. Afterwards, the ankle joint angle is averaged at each sample for all strides.

6. RESULTS

6.1. Ankle reference profile generator

To evaluate the efficiency of the adaptive reference algorithm, subject 1 was asked to walk on a treadmill at four different speeds: 1.6, 2, 2.4, and 3 Kilometers per hour.

For all sessions, the gait detection algorithm updates routines for the reference generator, e.g., the calculation for the step duration, the duration percentages of each gait sub-phase, and the ankle joint reference trajectory. The measured ankle joint angle, the reference ankle joint angle and angular velocity data were normalized with respect to the gait cycle, measured from one IC event to the next one, and the average was calculated thereafter. Each sub-phase is detected using the algorithm described in section 2.2 and each sub-phase phase

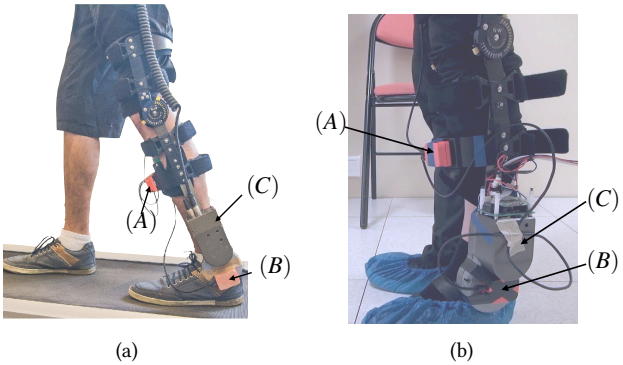

(a) (b)

Figure 6: On the left, a healthy subject wearing the system. On the right, the paretic patient wearing the system. The setup of the system is: (A) IMU used to estimate the angle between the shank and the vertical axis, (B) IMU measuring the translational accelerations, and (C) active-ankle-foot-orthosis with embedded encoders to measure the ankle joint angle.

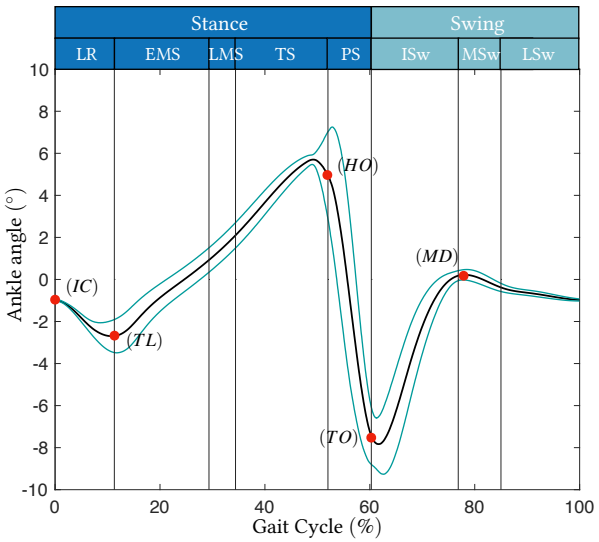

Figure 7: Mean ankle joint angle reference generated by the AARG algorithm during an unassisted session with a healthy subject. The cyan lines represent the standard deviation and the vertical lines dividing the gait cycle are the detected gait phases.

duration is then averaged for the whole session and normalized with respect to the gait cycle in order to calculate the mean proportions of the gait sub-phases. Figure 7 shows the mean ankle joint angle reference generated by the AARG algorithm during an unassisted session with a healthy subject while walking on a treadmill at 2 Kilometers per hour. It can be observed that all the sub-phases are correctly identified. The key points used for the AARG are highlighted in the figure. All the key points correspond to the description shown in Figure 1. The increased value of the standard deviation after the transition between the terminal stance (TS) and pre-swing (PS) sub-phases correspond to the high variability of the gait kinematics at every step.

Figure 8 shows the generated ankle profile and steps duration during the four sessions. It is worth noting, as it is shown in Figure 8a, that the ankle joint angle reference trajectory is similar during all sessions, independently of the gait speed, which makes the algorithm more robust with respect to changes in the step durations within a single or multiple session. The average step duration for each session is presented in Table 5. Figure 8b shows that the reference ankle joint velocity is updated with respect to the gait speed. However, the ankle joint kinematics changes slightly for different gait speeds and the amplitude of the ankle joint range of motion is reduced at the lowest speed while it is increased at the highest speed, as it can be seen in Figure 8c. For this reason, and in order to compare the results in similar conditions, the rest of the sessions, where the assistance is provided to the subjects, have been performed on the treadmill at a fixed speed of 2 Kilometers per hour. Furthermore, for the sessions with the patient, a slow walking speed of approximately 2 Kilometers per hour is requested for safety.

6.2. Experimental results with healthy subjects

The scalar gains a_i of the adaptation law (10) have been set for the first subject, using the protocol defined in 4.1 (Re-

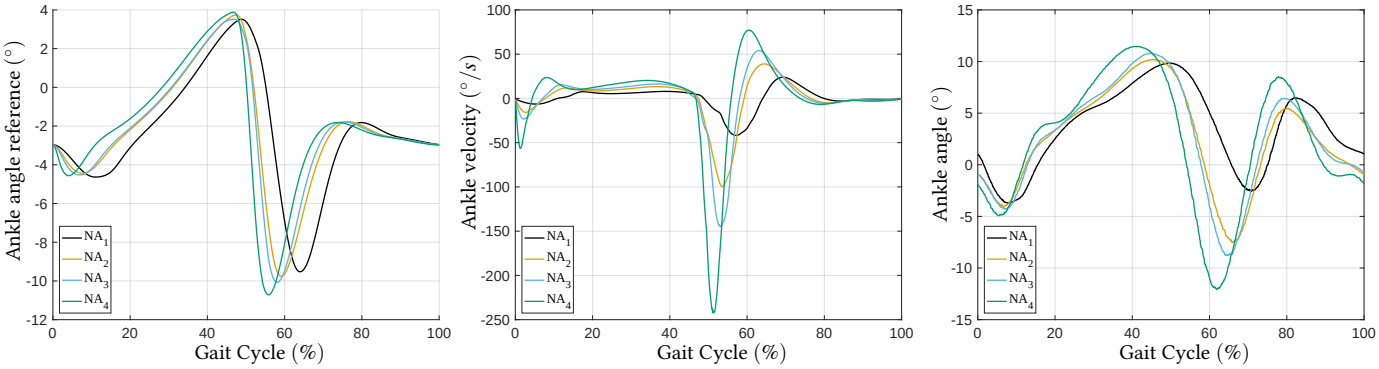

(a) Mean ankle joint angle reference. (b) Mean ankle joint velocity reference. (c) Mean real ankle joint angle.

Figure 8: Generated ankle profile and steps duration at four different walking speeds. A = assisted session, NA = no assistance session. Figure 8a and 8b show the mean ankle joint angle and velocity reference profiles for each session, normalized to the gait cycle. Figure 8c shows the mean ankle joint angle performed by the subject during each session, normalized to the gait cycle.

mark 2): $a_1 = a_2 = 0.002$, $a_3 = 0.01$, $a_4 = 1$, $a_5 = 0.00001$, $a_6 = 3$, and $a_7 = 2$. The controller's gains have been set to: $\kappa = 0.9$ and $\lambda = 7$ with all the adaptive parameters initialized to zero, and the ankle joint angle at the rest position $\theta_r = \frac{\pi}{2}$. These tuning gains values have been considered for all the subjects who participated in this study. The proposed controller was able to track the generated adaptive desired ankle trajectory profile within the first seconds and the error has decreased over time. The results for one assisted session for subject 1 are shown in Figure 9. The first 20 seconds of the tracking performance of the ankle joint angle and angular velocity, as well as the assistive torque delivered by the AAFO are shown in Figure 9a. The assistive torque presents an increasing peak value in the plantar flexion direction during terminal stance (TS), which represents an increasing assistance for push-off at the end of the stance phase. However, the assistance does not continue to increase after the 8th step, which means the system has reached stability. In Figure 9b, the performance of the adaptive parameters from equations (10) is shown for the complete session lasting 60 seconds. It can be seen that all parameters have converged to their final values, except for the stiffness parameter which is still updating. With an active wearer performing the experiments, the system is proved to be input-to-state stable. It means that the system's states remain bounded but do not converge to zero as it was the case with the asymptotic stability (passive wearer). Consequently, the adaptive parameters do not converge to constant values. Note that all adaptive parameters were able to converge to a final value when the system was tested in a passive condition (see [44]).

Using the gait phase detection algorithm shown in section 2.2, the assistive torque, the reference and the current ankle joint angles have been normalized with respect to the gait cycle. The results of an experimental session for the three subjects are shown in Fig 10. In Figures 10a, 10b, and 10c, the mean torques are shown for subject 1, 2, and 3, respectively; a positive torque represents a plantar-flexion assistance while a negative torque represents a dorsiflexion assistance. From Figures 10a and 10c, a predominately plantar flexion assistance can be observed due to the fact that the reference trajectory is more plantar-flexed than the normal ankle angle profile performed by subjects 1 and 3. Nevertheless, all subjects present an increased plantar-flexion assistance during the PS sub-phase, which corresponds to the push-off assistance. Since the ankle joint reference has a relatively smaller range of motion compared to that of the subjects, this push-off assistance is quickly reduced, or even changed to a dorsiflexion assistance as in the case of subject 2 (Figure 10b). During the swing phase, all the three healthy subjects have reported an assistance provided by the AAFO. This assistance is greater in the plantar-flexion direction, which is deliberate in order to assess the effectiveness of the system to modify the ankle joint angle even with healthy subjects. Hence, if the key-points in the AARG are adjusted, the assistance direction and magnitude can be manipulated. Furthermore, during the loading response (LR) sub-phase, the assistance provided for subjects 1 and 3 is provided in the dorsiflexion direction, as shown in Figures 10a and 10c. The percentage of the gait sub-phase durations relative to the whole gait cycle can be different for each stride, and for each subject. This can be seen in Figure 10, where the mean sub-phase duration percentage is represented by the vertical lines dividing the gait cycle into LR, MS, TS, PS, and swing sub-phases. Despite these different gait sub-phases and step durations for the different subjects participating in this study, the AARG was able to correctly update the generated trajectory and produce an ankle joint angle reference tailored for the subject profile.

Table 5: *Mean step duration (MSD) and standard deviations in milliseconds (ms) for unassisted sessions with Subject 1 on a treadmill at different walking speeds.*

	Session 1	Session 2	Session 3	Session 4
MSD	3630±158	2058±43	1670±50	1282±23

The assistive torque behavior is different from one subject to another but is consistent across all the sessions for each subject. This is shown in the left column of Figure 11, where the mean assistive torque provided by the AAFO and its standard deviation, normalized with respect to the gait cycle, for each

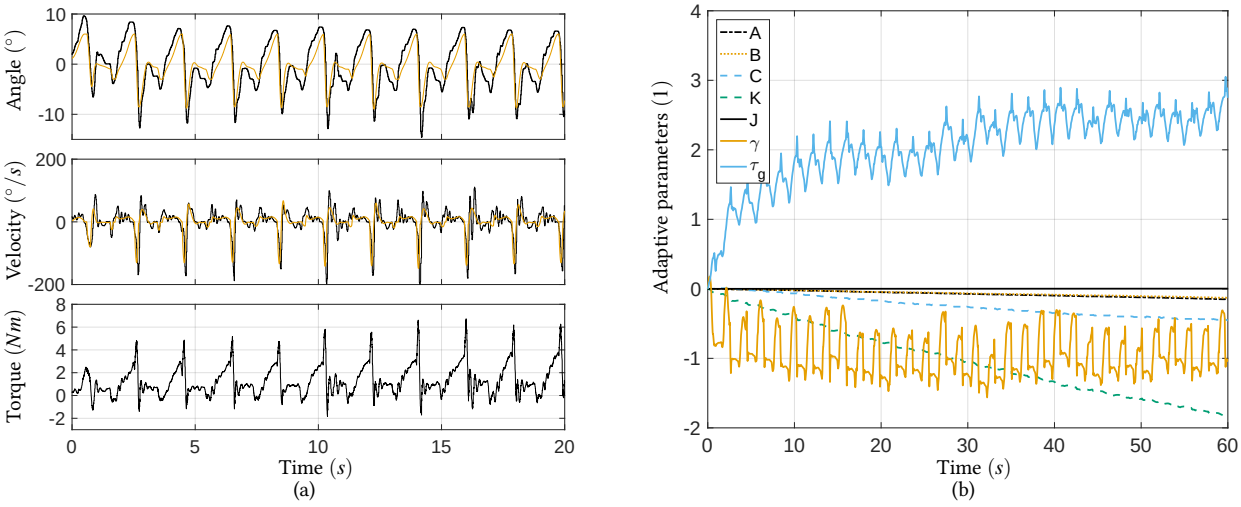

Figure 9: In 9a, the system's performance tracking the desired ankle joint angle profile during one session for subject 1 zoomed in for the first 20 seconds. In the top two plots, the yellow line represents the desired profile and the black line is the profile executed by the subject's ankle. In the bottom plot, the control torque delivered by the motor is presented. 9b, the system's adaptive parameters performance during the whole session.

assisted session are presented. It is worth noting that the assistive torque provided during the swing phase is not as large as the one generated during the stance phase, even though the position error is larger in the latter. This is mainly due to the fact that the torque generated from the ground reaction force is contributing to the total assistive torque.

The root-mean-square value of the position error is computed as well as its standard deviation. Table 6 shows the mean position error values for each subject and session, both with and without assistance. It can be observed that the tracking error is reduced by 55%, 44%, and 49% in average for subject 1, 2, and 3, respectively, when the assistive torque is provided. Furthermore, in the right column of Figure 11, the comparison of the normalized ankle joint angle and its reference for all the 6 sessions (3 sessions with assistance and 3 without) is shown for each subject. It can be observed that the normalized tracking error profile has a small standard deviation across all the assisted and unassisted sessions.

6.3. Experimental results with paretic patient

For the experiments with a paretic patient, 3 sessions without assistance and 3 sessions with assistance are conducted. All sessions are performed at a relatively slow self-selected walking speed for improved safety. One session consists of a 8 m walking on level ground with the first 5 steps used to intialize the AARG. A resting period of 1 minute is provided between sessions. The paretic patient suffered a stroke 6 years before the experiments and has received rehabilitation therapy at the Henri Mondor Hospital for 4 years. The patient had an absence of spasticity.No plantar flexor's stretch reflex was observed during the experiments. The age, weight, height and gender of the patient are given in Table 3. The scalar gains a_i of the adaptive law, equation (10), have been set for the patient (Remark 2): $a_1 = a_2 = 0.002$, $a_3 = 0.1$, $a_4 = 1$, $a_5 = 0.00001$, $a_6 = 2.5$, and $a_7 = 2$, the controller's gains have been set by trial and error as follows: $\kappa = 0.5$ and $\lambda = 6$ with all the adaptive parameters initialized to zero, and the ankle joint angle at the rest position $\theta_r = \frac{\pi}{2}$. As mentioned in 4.1, these tuning gains were defined in order to produce a slightly smaller assistive torque with respect to the one developed with healthy subjects for improved safety. The ankle joint key point values used for defining the AARG are presented in Table 4. These key point values generate an ankle joint angle reference profile that aims to increase the plantar flexion during the terminal stance (TS) sub-phase and to increase the dorsiflexion of the ankle joint at the end of the swing phase.

Table 6: *Position error in RMS for each session* $(error(^\circ) \pm std(^\circ))$. *A = assistance session, NA = no assistance session.*

Session	Subject 1	Subject 2	Subject 3
A 1	2.07±2.39	3.02±4.28	3.69±4.61
A 2	2.12±2.53	2.97±4.3	3.09±4.14
A 3	2.17±2.63	2.99±4.35	3.21±4.29
NA 1	5.22±3.45	4.49±3.94	4.43±3.92
NA 2	5.63±6.38	5.43±6.55	4.92±6.32
NA 3	6.88±6.65	6.44±6.07	6.33±6.57

Figure 12a shows, for one assisted session, the tracking performance for the ankle joint angle and angular velocity, as well as the assistive torque delivered by the AAFO. Due to the gait dynamics of the patient compared to the healthy subjects, the assistive torque presents chattering at some moments during the session. However, the system remains stable and the ankle joint angular error is reduced. In Figure 12b, the performance of the adaptive parameters is shown, similar to the healthy subject experiments; all the adaptive parameters from equations (10) converge to their final values, except for the stiffness parameter that keeps updating its value till the end of the session. Using the gait phase detection algorithm, the assistive torque, the reference and the current ankle joint angles have been normalized with respect to the gait cycle. The

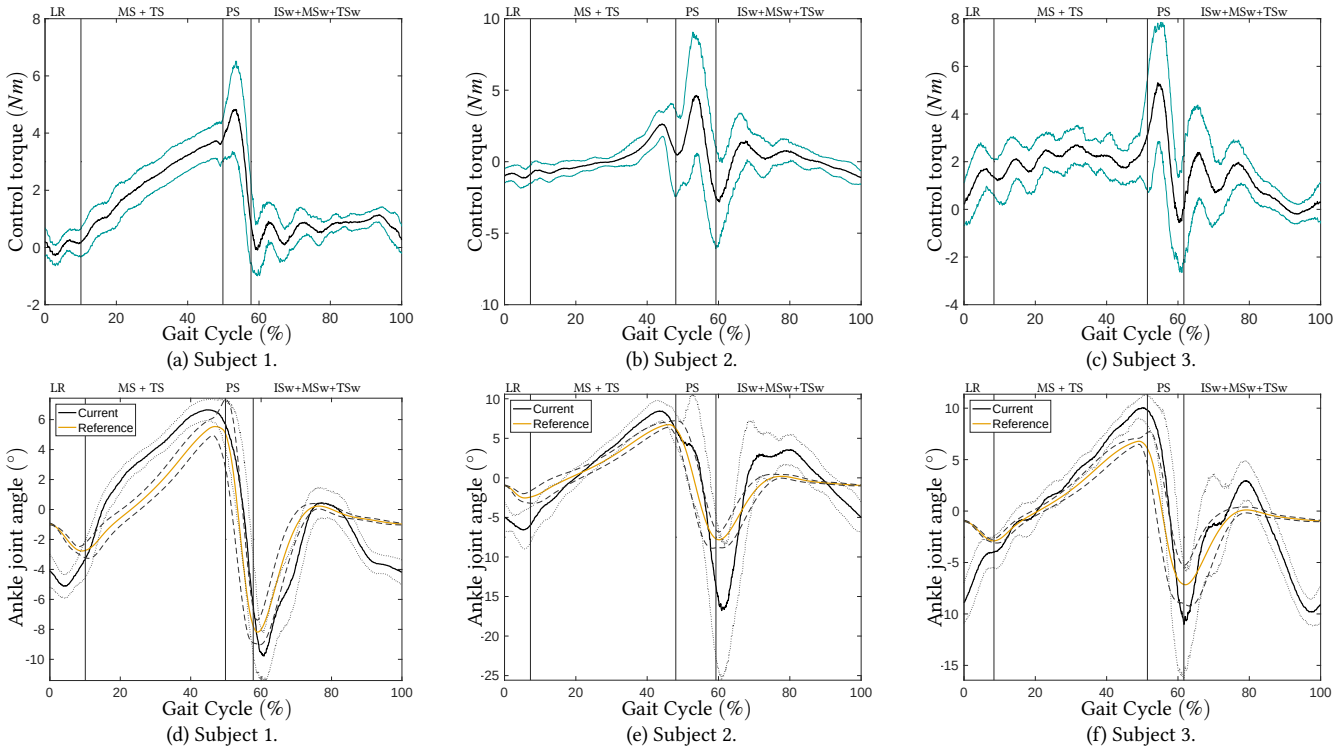

(a) Subject 1. (b) Subject 2. (c) Subject 3.

(d) Subject 1. (e) Subject 2. (f) Subject 3.

Figure 10: In 10a, 10b, and 10c, the system's normalized mean assistive torque for one assisted session of each subject. The black lines represent the mean values and the cyan lines represent the standard deviations about the mean values. In 10d, 10e, and 10f, the mean ankle joint reference and current angles. The black lines represent the current ankle joint angles, the yellow lines represent the reference trajectories, the dotted and dashed grey lines represent the standard deviations for the current and reference ankle joint profiles, respectively. In all figures the vertical lines represent the divisions between the gait sub-phases relevant to the ankle reference updates.

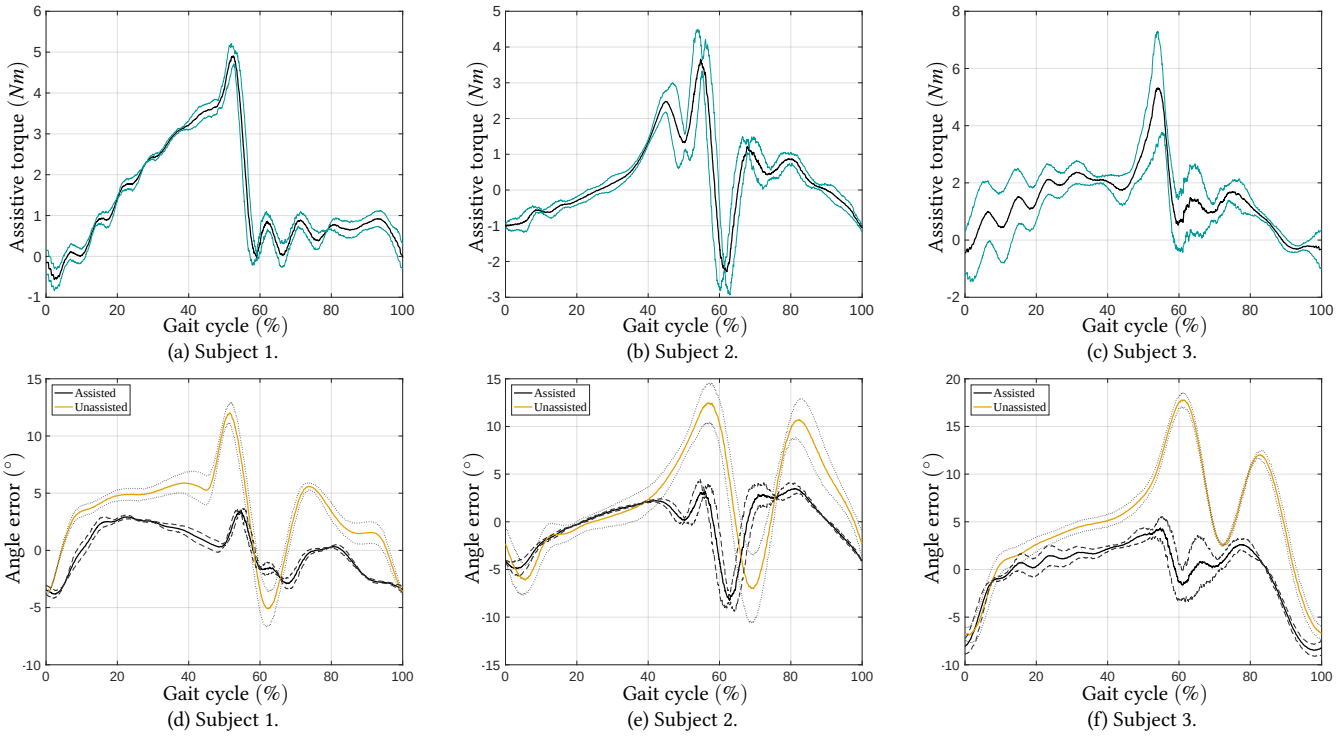

(a) Subject 1. (b) Subject 2. (c) Subject 3.

(d) Subject 1. (e) Subject 2. (f) Subject 3.

Figure 11: In 11a, 11b, and 11c, the mean normalized assistive torque for all the 3 sessions for each healthy subject. The black lines represent the mean values and the cyan lines represent the standard deviations from the mean. In 11d, 11e, and 11f, the mean normalized ankle joint errors for the 3 sessions with assistance and the 3 sessions without assistance, for each subject. The black lines represent the assisted scenario and the yellow lines represent the unassisted scenario. The dashed and dotted grey lines represent the standard deviations from the mean for the assisted and unassisted scenarios, respectively.

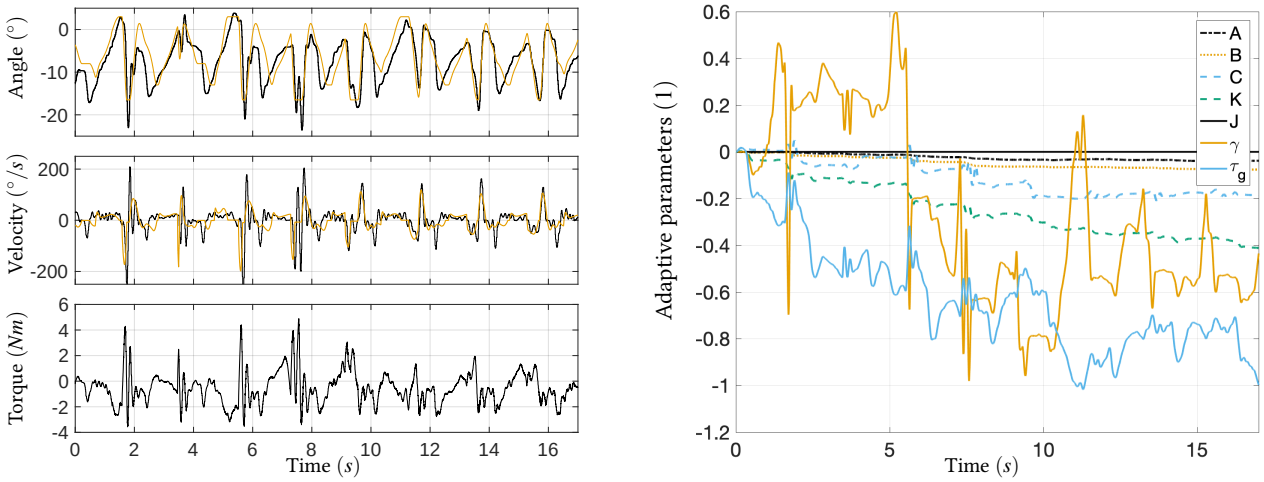

(a) System performance

(b) Adaptive parameters

Figure 12: In 12a, the system's performance tracking the desired ankle joint angle profile during one session for the patient. In the top two plots, the light grey line represents the desired profile and the solid black line is the profile executed by the patient's ankle. In the bottom plot, the control torque delivered by the motor is presented. In 12b, the system's adaptive parameters performance during the same session.

results of one assisted and one unassisted sessions are shown in Fig 13b and Fig 13a, respectively. From these figures, a comparison between the normalized ankle joint angle profiles during the assisted and unassisted sessions can be done. On the one hand, for the unassisted session, the patient shows a gait cycle with a predominate plantar flexion, specially at the end of the swing phase and during the loading response sub-phase where the foot plantar flexes excessively, probably due to co-contraction between the plantar flexion and the dorsiflexion muscle groups. However, due to the limited range of motion (ROM) of the ankle joint during terminal stance (TS) and pre-swing (PS) sub-phases, the patient does not show sufficient push-off movement. On the other hand, for the assisted session, the ankle joint angle profile shows an increased dorsiflexion during all the gait cycle and the plantar flexion motion at the loading response sub-phase is reduced. Likewise, an increased ROM of the ankle joint during the TS and PS sub-phases (from 7.86±1.98° to 18.09±3.83°) results in an improved push-off motion while increasing the maximum dorsiflexion achieved during the swing phase (from -5.59±1.46° to 0.61±2.03°). Finally, the standard deviation of the average error decreased from ±5.00° in the unassisted experiments, to ±3.70° in the assisted ones. This reduction in the standard deviation is not evident in Fig. 13, the reason for this is that the ankle joint angle profile is modified both in time and space, i.e., the proportions of the gait sub-phases relatively to the gait cycle are modified and the normalization of the ankle joint angle profile with respect to the gait cycle reflects this change with an increased standard deviation.

In Figure 13c, the mean torque across all three assisted sessions is shown, as well as its standard deviation. It can be observed a relatively higher standard deviation value across the gait cycle with respect to the one observed with the healthy subjects, mainly due to the variations between each step of the paretic leg of the patient. In Figure 13d, a comparison between the mean ankle joint angle profiles for the assisted and unassisted sessions is shown. It can be seen that the maximum plantar flexion angle prior to the swing phase is increased, effectively contributing to push-off. Furthermore, the maximum dorsiflexion angle during the swing phase is increased, reducing the risk of foot-drop.

The root-mean-square value of the position error is computed as well as the standard deviation and classified in four gait groups relative to the sub-phases: loading response (LR), roll over (MS plus TS), push-off (PS), and swing (ISw plus MSw plus TSw). Figure 14 shows the position error values for each session, both with and without assistance, classified by the aforementioned gait groups. It can be observed that the normalized tracking error is reduced by 51%, 77%, 74%, and 60% for the loading response, roll over, push-off, and swing gait groups, respectively, when the assistive torque is provided.

6.4. *Comparison with state-of-the-art*

In a previous study [44], the adaptive controller was assessed only during the swing phase with a healthy subject. While the proposed method showed satisfactory tracking performances over time, the adaptive parameters were not able to converge to their final values due to the discontinuous desired trajectory and the intermittent assistance being provided. In a second study [45], the desired trajectory was defined for the whole gait cycle and the assistance was provided continuously. However, the gait pace had to be synchronized with an audible cue in order to provide an appropriate assistance. In this paper, the adaptive controller was tested with three healthy subjects and one paretic patient. Furthermore, the desired trajectory adapts to the walking speed and gait pace of the wearer.

In the literature, one can note several ankle assessment techniques [52]. For example, the range of motion (ROM) of the ankle joint is one important criterion as it reflects the efficiency of the gait, and the ankle strength can assess the ability to generate movement. The AAFO used in this paper is able to measure the ankle ROM so the results of the kinetic data from

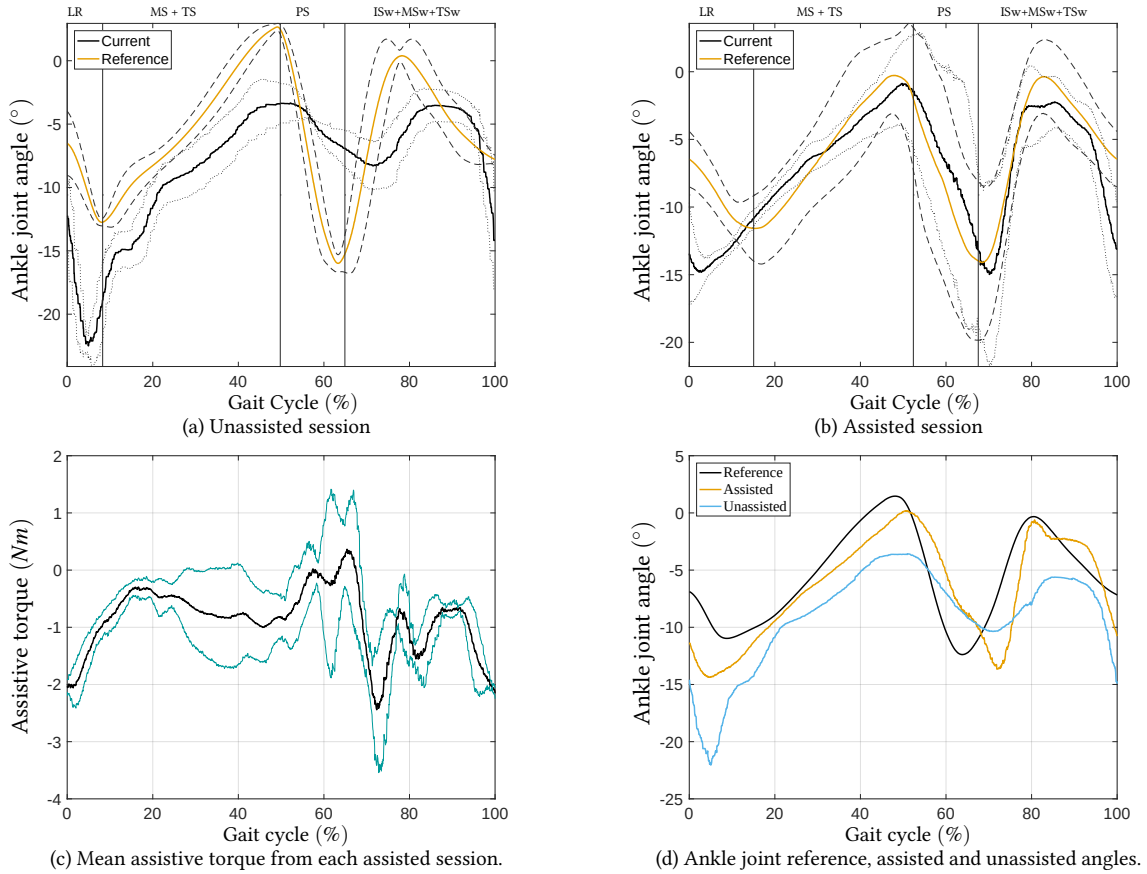

(a) Unassisted session

(b) Assisted session

(c) Mean assistive torque from each assisted session.

(d) Ankle joint reference, assisted and unassisted angles.

Figure 13: In 13a and 13b, the normalized ankle joint angles for one unassisted and one assisted session with the patient; in dotted and dashed grey lines the standard deviation for the current and reference ankle profiles, respectively. In 13c, the mean normalized assistive torque from the three assisted sessions; in cyan the standard deviation from the mean. In 13d, a comparison between the ankle joint reference, and real angles from the 3 assisted and the 3 unassisted sessions with the patient.

the paretic subject of the present study are compared with the state-of-the-art.

In [32], two foot drop patients were recruited. It is reported an elimination of foot slap occurrences at slow and self-selected walking speeds. During the swing phase, a variable impedance controller was able to increase the amount of the ROM, as compared to the constant impedance controller, by 200% and 37% for slow and self-selected gait speeds, respectively. However, no quantitative information is given when comparing to an unassisted scenario. Results obtained by Blaya and Herr can be compared to the results obtained in this study. For instance, the adaptive controller proposed in this paper was able to increase the ROM during the swing phase by 98%, as compared to the unassisted scenario. The difference between the results could be attributed to the difference in strategy during the swing phase; i.e., in [32], the controller was tuned to promote the dorsiflexion velocity of the ankle joint in the early swing phase matching the unaffected side, without a prior knowledge of the maximum dorsiflexion angle during the swing phase.

7. DISCUSSION

Traditional proportional, integral derivative (PID) controllers have been widely used with robotic orthoses in the rehabilitation environment [25–28, 35]. While such controllers can be used to track a predefined trajectory for the ankle joint, they usually lack the performance achieved by model based controllers. However, these control strategies require accurate knowledge of the system's parameters, i.e. wearer-active orthosis' parameters, to calculate the needed assistive torque might not be adequate in a rehabilitation environment. This is due to the fact that the identification process has to be done prior to each session and with each subject, which is time and effort consuming. Furthermore, unconsidered external perturbations could increase the risk of inappropriate assistance, reduce the rehabilitation benefits, or even cause injuries. Therefore, an adaptive model based control strategy presents a clear advantage over the classical PID and traditional model based control approaches even if more scalar gains need to be tuned for the controller.

In addition, the synchronization between the ankle joint profile reference and the gait cycle is paramount for providing appropriate assistance. For this reason, an adaptive reference trajectory is proposed as a function of the walking speed of

the wearer. The purpose of this study is to assist the gait in order to reduce the effects of the pathology described as foot drop and to enhance the effects of the push-off at the stance phase.

In this work, the results show satisfactory tracking and a relatively fast convergence of the adaptive parameters without any prior system identification, making the proposed approach suitable for rehabilitation purposes.

While IMU sensors can be used to detect the stance and swing phases of the gait cycle [53], the FSR sensors are able to provide a better estimation of the gait events, particularly those of the stance phase; i.e., the initial contact, toe-landing, heel-off, and toe-off events. Since such events could be linked to the ankle joint profile during the gait cycle while the controller approach required the estimation of the ground reaction forces, three FSR sensors per feet were used. However, it should be noted that a small delay in the detection of the IC event was observed. Therefore, the combined use of the IMU and FSR sensors proved to be effective for an accurate detection of the gait phases. Nevertheless, the IMUs contain information about the kinematics of the gait cycle that could be used to further improve the gait phase detection algorithm with subjects suffering from heavy gait difficiencies for example. Therefore, the robustness of such an enhanced algorithm will be studied in a future work.

This study will also be extended in different perspectives. First, this proposed control strategy can be enhanced and applied for other joints, e.g., knee and hip, while using lower limbs exoskeletons. This will require to define the profile trajectories for each joint and implement an adaptive joint reference generator in order to allow the user to self-select the walking speed. Based on this, even an upper body application can be considered for a grasping and reaching task. Secondly, since the proposed control is proved to be input-to-state stable with respect to the muscle generated torque, a hybrid approach that implements functional electrical stimulation will be studied. Thirdly, the effects of the assistance provided by the AAFO to spastic paretic patients will be studied.

Relying on a predefined desired trajectory may not be comfortable for subjects due to the fact that patient profiles are very different. Therefore, the ankle joint reference needs to be updated online and it should be adapted with respect to the wearer's walking speed and the gait phase durations. The former is satisfied by adjusting the reference velocity and the latter by adjusting the different proportions on the sub-phase durations. The experiment results show that the proposed adaptive reference algorithm is able to generate a suitable ankle joint profile tailored to each subject at his/her own walking speed. Furthermore, by setting different ankle reference key points (Table 1 compared to Table 4) the assistive torque provided for each subject can be adjusted. Moreover, only ground reaction forces and shank acceleration in the longitudinal axis are used for the AARG algorithm, making the system portable and lightweight.

The system proved to be stable for its use in a clinical environment. The proposed adaptive reference algorithm is able to generate an adapted ankle joint profile despite the deficiencies

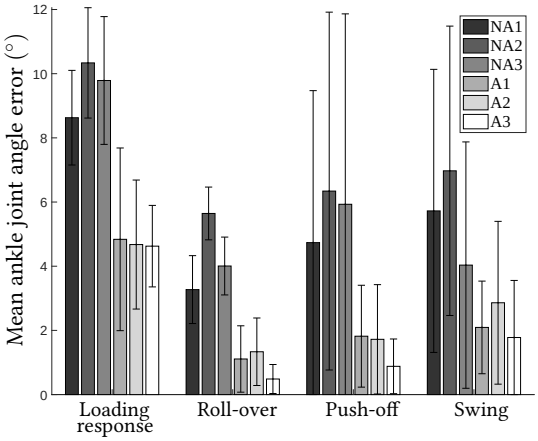

Figure 14: Mean ankle joint angle position errors across the gait cycle for the assisted and unassisted sessions with patient.

in the ankle joint during the gait of the paretic patient. The obtained results showed that an ankle reference profile generated in real time based on the current state of the wearer's gait could potentially assist the ankle joint of paretic subjects and prevent eventual falls due to foot drop effects. The assistance provided by the AAFO can increase the ankle dorsiflexion during the swing phase; which can correct foot drop even in the presence of co-contraction, and increase the ankle plantar flexion during push-off.

References

[1] W. L. Anderson, B. S. Armour, E. A. Finkelstein, J. M. Wiener, Estimates of state-level health-care expenditures associated with disability, Public Health Reports 125 (1) (2010) 44–51.

[2] E. B. Brokaw, D. Nichols, R. J. Holley, P. S. Lum, Robotic therapy provides a stimulus for upper limb motor recovery after stroke that is complementary to and distinct from conventional therapy, Neurorehabilitation and Neural Repair 28 (4) (2014) 367–376.

[3] V. Klamroth-Marganska, J. Blanco, K. Campen, A. Curt, V. Dietz, T. Ettlin, M. Felder, B. Fellinghauer, M. Guidali, A. Kollmar, et al., Three-dimensional, task-specific robot therapy of the arm after stroke: a multicentre, parallel-group randomised trial, The Lancet Neurology 13 (2) (2014) 159–166.

[4] P. S. Lum, C. G. Burgar, P. C. Shor, M. Majmundar, M. Van der Loos, Robot-assisted movement training compared with conventional therapy techniques for the rehabilitation of upper-limb motor function after stroke, Archives of Physical Medicine and Rehabilitation 83 (7) (2002) 952–959.

[5] W. H. Chang, Y.-H. Kim, Robot-assisted therapy in stroke rehabilitation, Journal of Stroke 15 (3) (2013) 174.

[6] X. Xie, H. Sun, Q. Zeng, P. Lu, Y. Zhao, T. Fan, G. Huang, Do patients with multiple sclerosis derive more benefit from robot-assisted gait training compared with conventional walking therapy on motor function? A meta-analysis, Frontiers in Neurology 8 (260) (2017) 9.

[7] S. Masiero, M. Armani, G. Ferlini, G. Rosati, A. Rossi, Randomized trial of a robotic assistive device for the upper extremity during early inpatient stroke rehabilitation, Neurorehabilitation and Neural Repair 28 (4) (2014) 377–386.

[8] S. E. Fasoli, H. I. Krebs, J. Stein, W. R. Frontera, R. Hughes, N. Hogan, Robotic therapy for chronic motor impairments after stroke: Follow-up results, Archives of Physical Medicine and Rehabilitation 85 (7) (2004) 1106–1111.

[9] M. Zhang, T. C. Davies, S. Xie, Effectiveness of robot-assisted therapy on ankle rehabilitation–a systematic review, Journal of Neuroengineering and Rehabilitation 10 (1) (2013) 1.

[10] L. Marchal-Crespo, D. J. Reinkensmeyer, Review of control strategies for robotic movement training after neurologic injury, Journal of Neuroengineering and Rehabilitation 6 (1) (2009) 15.

[11] B. S. Rupal, S. Rafique, A. Singla, E. Singla, M. Isaksson, G. S. Virk, Lower-limb exoskeletons: Research trends and regulatory guidelines in medical and non-medical applications, International Journal of Advanced Robotic Systems 14 (6) (2017) 27.

[12] S. Mohammed, Y. Amirat, H. Rifai, Lower-limb movement assistance through wearable robots: State of the art and challenges, Advanced Robotics 26 (1-2) (2012) 1–22.

[13] H. Herr, Exoskeletons and orthoses: classification, design, challenges and future directions, Journal of Neuroengineering and Rehabilitation 6 (1) (2009) 9.

[14] W. Huo, S. Mohammed, J. C. Moreno, Y. Amirat, Lower limb wearable robots for assistance and rehabilitation: A state of the art, Systems Journal 10 (3) (2016) 1068–1081.

[15] K. A. Shorter, J. Xia, E. T. Hsiao-Wecksler, W. K. Durfee, G. F. Kogler, Technologies for powered ankle-foot orthotic systems: Possibilities and challenges, Transactions on Mechatronics 18 (1) (2013) 337–347.

[16] S. M. Cain, K. E. Gordon, D. P. Ferris, Locomotor adaptation to a powered ankle-foot orthosis depends on control method, Journal of neuroengineering and rehabilitation 4 (1) (2007) 1.

[17] A. W. Boehler, K. W. Hollander, T. G. Sugar, D. Shin, Design, implementation and test results of a robust control method for a powered ankle foot orthosis (AFO), International conference on Robotics and automation (ICRA) (2008) 2025–2030.

[18] R. Jimenez-Fabian, O. Verlinden, Review of control algorithms for robotic ankle systems in lower-limb orthoses, prostheses, and exoskeletons, Medical Engineering & Physics 34 (4) (2011) 397–408.

[19] K. E. Gordon, C. R. Kinnaird, D. P. Ferris, Locomotor adaptation to a soleus EMG-controlled antagonistic exoskeleton, Journal of Neurophysiology 109 (7) (2013) 1804–1814.

[20] J. C. Pérez-Ibarra, A. A. Siqueira, Comparison of kinematic and EMG parameters between unassisted, fixed-and adaptive-stiffness robotic-assisted ankle movements in post-stroke subjects, International Conference on Rehabilitation Robotics (ICORR) (2017) 461–466.

[21] D. P. Ferris, K. E. Gordon, G. S. Sawicki, A. Peethambaran, An improved powered ankle–foot orthosis using proportional myoelectric control, Gait & Posture 23 (4) (2006) 425–428.

[22] M. Dzahir, N. Nor, A. Azaman, M. Hussein, M. M. Dzahir, Pneumatic muscles actuated lower-limb orthosis model verification with actual human muscle activation patterns, MATEC Web of Conferences 135 (2017) 00061.

[23] J.-i. Furukawa, T. Noda, T. Teramae, J. Morimoto, Human movement modeling to detect biosignal sensor failures for myoelectric assistive robot control, Transactions on Robotics 33 (4) (2017) 846–857.

[24] M. Zhang, J. Cao, S. Q. Xie, G. Zhu, X. Zeng, X. Huang, Q. Xu, A preliminary study on robot-assisted ankle rehabilitation for the treatment of drop foot, Journal of Intelligent & Robotic Systems (2017) 1–9.

[25] M. A. Holgate, A. W. Bohler, T. G. Suga, Control algorithms for ankle robots: A reflection on the state-of-the-art and presentation of two novel algorithms, International Conference on Biomedical Robotics and Biomechatronics (2008) 97–102.

[26] J. Hitt, A. M. Oymagil, T. Sugar, K. Hollander, A. Boehler, J. Fleeger, Dynamically controlled ankle-foot orthosis (DCO) with regenerative kinetics: incrementally attaining user portability, International Conference on Robotics and Automation (ICRA) (2007) 1541–1546.

[27] J. Ward, T. Sugar, J. Standeven, J. R. Engsberg, Stroke survivor gait adaptation and performance after training on a powered ankle foot orthosis, International Conference on Robotics and Automation (ICRA) (2010) 211–216.

[28] I. Veneva, N. Ferreira, Adaptive system for control of active ankle-foot orthosis and gait analysis, in: Mathematical Methods in Engineering, Springer, 153–163, 2014.

[29] M. Noël, B. Cantin, S. Lambert, C. M. Gosselin, L. J. Bouyer, An electro-hydraulic actuated ankle foot orthosis to generate force fields and to test proprioceptive reflexes during human walking, Transactions on Neural Systems and Rehabilitation Engineering 16 (4) (2008) 390–399.

[30] Y. Ren, Y.-N. Wu, C.-Y. Yang, T. Xu, R. Harvey, L.-Q. Zhang, Developing a wearable ankle rehabilitation robotic device for in-bed acute stroke rehabilitation, Transactions on neural systems and rehabilitation engineering 25 (6) (2016) 589–596.

[31] F. el Zahraa Wehbi, W. Huo, Y. Amirat, M. El Rafei, M. Khalil, S. Mohammed, Active impedance control of a knee-joint orthosis during swing phase, International Conference on Rehabilitation Robotics (ICORR) (2017) 435–440.

[32] J. A. Blaya, H. Herr, Adaptive control of a variable-impedance ankle-foot orthosis to assist drop-foot gait, Transactions on Neural Systems and Rehabilitation Engineering 12 (1) (2004) 24–31.

[33] M. J. Lawn, M. Takashima, M. Ninomiya, J. Yu, K. Soma, T. Ishimatsu, Development of an actuation system for a rotary hydraulic brake on a low cost light weight knee-ankle-foot orthosis, Sensors (2015) 1–4.

[34] A. Roy, H. I. Krebs, J. E. Barton, R. F. Macko, L. W. Forrester, Anklebot-assisted locomotor training after stroke: A novel deficit-adjusted control approach, in: International Conference on Robotics and Automation (ICRA), IEEE, 2175–2182, 2013.

[35] A. Roy, H. I. Krebs, K. Iqbal, N. R. Macko, R. F. Macko, L. W. Forrester, Facilitating push-off propulsion: A biomechanical model of ankle robotics assistance for plantarflexion gait training in stroke, International Conference on Biomedical Robotics and Biomechatronics (2014) 656–663.

[36] J. Ghan, R. Steger, H. Kazerooni, Control and system identification for the Berkeley lower extremity exoskeleton (BLEEX), Advanced Robotics 20 (9) (2006) 989–1014.

[37] K. A. Shorter, G. F. Kogler, E. Loth, W. K. Durfee, E. T. Hsiao-Wecksler, A portable powered ankle-foot orthosis for rehabilitation, Journal of rehabilitation research and development 48 (4) (2011) 459–472.

[38] M. N. A. Ab Patar, A. F. Said, J. Mahmud, A. P. A. Majeed, M. A. Razman, System integration and control of dynamic ankle foot orthosis for lower limb rehabilitation, International Symposium on Technology Management and Emerging Technologies (ISTMET) (2014) 82–85.

[39] V. Arnez-Paniagua, W. Huo, I. Colorado-Cervantes, S. Mohammed, Y. Amirat, A hybrid approach towards assisting ankle joint of paretic patients, IFES Hybrid Approaches to FES (2016) 4.

[40] H. Zhu, J. Doan, C. Stence, G. Lv, T. Elery, R. Gregg, Design and validation of a torque dense, highly backdrivable powered knee-ankle orthosis, International Conference Robotic Automation (ICRA) (2017) 7.

[41] Y.-L. Park, B.-r. Chen, D. Young, L. Stirling, R. J. Wood, E. Goldfield, R. Nagpal, Bio-inspired active soft orthotic device for ankle foot pathologies, Intelligent Robots and Systems (IROS) (2011) 4488–4495.

[42] D. K. Sommerfeld, E. U.-B. Eek, A.-K. Svensson, L. W. Holmqvist, M. H. von Arbin, Spasticity after stroke: its occurrence and association with motor impairments and activity limitations, Stroke 35 (1) (2004) 134–139.

[43] M. Vinti, A. Couillandre, J. Hausselle, N. Bayle, A. Primerano, A. Merlo, E. Hutin, J.-M. Gracies, Influence of effort intensity and gastrocnemius stretch on co-contraction and torque production in the healthy and paretic ankle, Clinical Neurophysiology 124 (3) (2013) 528–535.

[44] V. Arnez-Paniagua, H. Rifai, S. Mohammed, Y. Amirat, Adaptive control of an actuated ankle foot orthosis for foot-drop correction, International Federation of Automatic Control (IFAC) (2017) 1420–1425.

[45] V. Arnez-Paniagua, H. Rifaï, Y. Amirat, S. Mohammed, Adaptive control of an actuated-ankle-foot-orthosis, International Conference on Rehabilitation Robotics (ICORR) (2017) 1584–1589.

[46] D. A. Winter, Biomechanics and motor control of human movement, John Wiley & Sons, 2009.

[47] K. Kong, M. Tomizuka, A gait monitoring system based on air pressure sensors embedded in a shoe, Transactions on mechatronics 14 (3) (2009) 358–370.

[48] E. Hutin, D. Pradon, F. Barbier, B. Bussel, J.-M. Gracies, N. Roche, Walking velocity and lower limb coordination in hemiparesis, Gait and Posture 36 (2) (2012) 205–211.

[49] J. Son, S. Hwang, Y. Kim, An EMG-based muscle force monitoring system, Journal of mechanical science and technology 24 (10) (2010) 2099–2105.

[50] H. Khalil, Nonlinear systems, Prentice Hall, 2002.

[51] J.-J. Slotine, L. Weiping, Adaptive manipulator control: A case study, Transactions on Automatic Control 33 (11) (1988) 995–1003.

[52] M. Zhang, T. C. Davies, Y. Zhang, S. Xie, Reviewing effectiveness of ankle assessment techniques for use in robot-assisted therapy, Journal of rehabilitation research and development 51 (4) (2014) 517–534.

[53] W. Huo, V. Arnez-Paniagua, M. Ghedira, Y. Amirat, Adaptive FES Assistance Using a Novel Gait Phase Detection Approach, in: IEEE/RSJ International Conference on Intelligent Robots and Systems, IROS, 2018.